BIOCHEMISTRY
including biophysical chemistry & molecular biology

ARTICLE

pubs.acs.org/biochemistry

Structures of Glycosylated Mammalian Glutaminyl Cyclases Reveal Conformational Variability near the Active Center

David Ruiz-Carrillo,[†,‡] Birgit Koch,[†] Christoph Parthier,[‡] Michael Wermann,[†] Tresfore Dambe,[§] Mirko Buchholz,[†] Hans-Henning Ludwig,[†] Ulrich Heiser,[†] Jens-Ulrich Rahfeld,[†] Milton T. Stubbs,[*,‡,∥] Stephan Schilling,[*,†] and Hans-Ulrich Demuth[†]

[†]Probiodrug AG, Weinbergweg 22, D-06120 Halle (Saale), Germany

[‡]Institut für Biochemie und Biotechnologie, Martin-Luther-Universität Halle-Wittenberg, Kurt-Mothes-Strasse 3, D-06120 Halle (Saale), Germany

[§]PSF AG, Robert-Roessle-Strasse 10, D-13092 Berlin, Germany

[∥]Mitteldeutsches Zentrum für Struktur und Dynamik der Proteine (MZP), Martin-Luther-Universität Halle-Wittenberg, D-06099 Halle (Saale), Germany

Supporting Information

ABSTRACT: Formation of N-terminal pyroglutamate (pGlu or pE) from glutaminyl or glutamyl precursors is catalyzed by glutaminyl cyclases (QC). As the formation of pGlu-amyloid has been linked with Alzheimer's disease, inhibitors of QCs are currently the subject of intense development. Here, we report three crystal structures of N-glycosylated mammalian QC from humans (hQC) and mice (mQC). Whereas the overall structures of the enzymes are similar to those reported previously, two surface loops in the neighborhood of the active center exhibit conformational variability. Furthermore, two conserved cysteine residues form a disulfide bond at the base of the active center that was not present in previous reports of hQC structure. Site-directed mutagenesis suggests a structure-stabilizing role of the disulfide bond. At the entrance to the active center, the conserved tryptophan residue, W^{207}, which displayed multiple orientations in previous structure, shows a single conformation in both glycosylated human and murine QCs. Although mutagenesis of W^{207} into leucine or glutamine altered substrate conversion significantly, the binding constants of inhibitors such as the highly potent PQ50 (PBD150) were minimally affected. The crystal structure of PQ50 bound to the active center of murine QC reveals principal binding determinants provided by the catalytic zinc ion and a hydrophobic funnel. This study presents a first comparison of two mammalian QCs containing typical, conserved post-translational modifications.

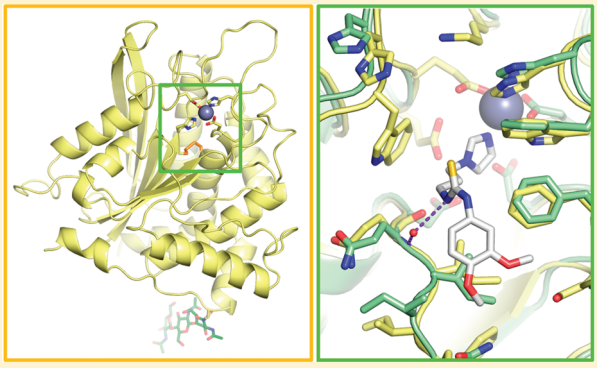

Glutaminyl cyclases (QC), which catalyze the formation of pyroglutamic acid (pGlu) at the N-terminus of several peptides and proteins,[1−4] have been isolated from animals, plants, and bacteria. Although the proteins from plants and animals are similar with respect to catalytic activity, they display widely differing structures.[5,6] In contrast, the bacterial and plant QCs appear to share a common ancestor.[7,8] In mammals, QCs catalyze the formation of pGlu-peptides from N-terminal Gln-precursors of hormones such as TRH (thyrotropin-releasing hormone), GnRH (gonadotropin-releasing hormone), neurotensin, or gastrin within the regulated secretory pathway.[9,10] Moreover, the enzymes have been shown to catalyze the formation of pGlu from N-terminal glutamyl (Glu) precursors.[11,12] Such activity makes QCs potential candidates for the formation of pGlu-modified amyloid peptides in Alzheimer's disease (AD) or the familial British and Danish dementias. Inhibition of QC attenuates AD-like symptoms in mice, establishing QC as a focus for drug development.[13]

Mammalian QCs are zinc-dependent glycoproteins.[14,15] The structure of human QC exhibits a typical α/β-hydrolase fold whose characteristic features are a central six-stranded β-sheet surrounded by α-helices.[5] Structural comparisons of the active centers of human QC and prototype aminopeptidases of the clan MH strongly support the hypothesis of a common ancestor of QC and bacterial dizinc aminopeptidases,[5] as suggested on the basis of homology searches.[16]

Although previous structural analyses of human QC[5,17] have yielded important insights into structure−activity relationships (SARs) of the enzyme, a number of earlier experimental findings are not reflected in these structures. Previous studies demonstrated discrepancies in the activities of hQC expressed in yeast and *Escherichia coli*[18] (Table S1 of the Supporting Information);

Received: February 18, 2011
Revised: May 19, 2011
Published: June 14, 2011

notably, mammalian QCs purified from porcine or bovine pituitary have been described as glycoproteins.[10,19] Moreover, hQC exhibits a slow inactivation in the presence of reducing agents.[18] Here we present the crystal structure determinations of both human and murine QCs expressed recombinantly in the yeast *Pichia pastoris*, revealing for the first time significant loop rearrangements in the neighborhood of the active center. In addition, we report the cocrystal structure of mQC in the presence of the potent QC inhibitor PQ50 (PBD150), shedding light on determinants of inhibitor binding.

MATERIALS AND METHODS

Materials. *E. coli* strain DH5α was applied for all cloning procedures. *P. pastoris* strain X33 (AOX1, AOX2) was used for the expression of the different hQC variants. Yeast was grown, transformed, and analyzed according to the manufacturer's instructions (Invitrogen, Karlsruhe, Germany). The glutaminyl peptides were obtained from Bachem (Bubendorf, Switzerland) or synthesized as described previously.[20] Recombinant pyroglutamyl aminopeptidase (pGAP) from *Bacillus amyloliquefaciens* was purchased from Qiagen (Hilden, Germany) and bovine liver glutamic acid dehydrogenase (GDH) from Sigma-Aldrich (Steinheim, Germany). Imidazole, benzimidazole, and cysteamine were purchased from Sigma-Aldrich. The low-salt LB medium required for propagation of *E. coli* and the buffered glycerol complex medium (BMGY) or buffered methanol complex medium (BMMY) as well as the yeast extract peptone dextrose (YPDS) agar, which are required for propagation of yeast, were prepared according to the Pichia manual and "Fermentation process guidelines" (Invitrogen).

Cloning Procedures. The hQC cDNA was inserted into yeast expression vector pPICZαB (Invitrogen) via the *Pst*I and *Not*I restriction sites. Additionally, an N-terminal His_6 tag was introduced using primers C_s (sense) and C_{as} (antisense) (Table S2 of the Supporting Information). Mutations in human QC were introduced by PCR-mediated site-directed mutagenesis according to standard PCR techniques using the appropriate primer pairs listed in Table S2. Following whole-plasmid amplification, the parent DNA was digested using *Dpn*I (Quik-change II site-directed mutagenesis kit, Stratagene, Santa Clara, CA). The cDNA sequence was verified by DNA sequencing, applying the primer S_s (W^{207}) or S_{as} (C^{139}, C^{164}). Murine QC was cloned as described elsewhere;[15] briefly, the cDNA was inserted via the *Xho*I and *Xba*I restriction sites into yeast expression vector pPICZαA without addition of an N-terminal His_6 tag.

Transformation of *P. pastoris* and Miniscale Expression. Plasmid DNA was amplified in *E. coli* strain DH5α, purified (Plasmid Miniprep Kit, Qiagen), and linearized using *Pme*I; 1−5 μg of DNA was applied for transformation of competent yeast cells [*P. pastoris* strain X33 (AOX1, AOX2)] by electroporation according to the manufacturer's instructions (Bio-Rad, Munich, Germany). Yeast was grown, transformed, and analyzed according to the manufacturer's instructions (Invitrogen). Selection of transgenics was achieved on YPDS plates containing 150 μg/mL Zeocin. Yeast cells were screened for protein expression as described previously.[15] To confirm the insertion of the correct hQC mutant, genomic DNA was prepared according to standard molecular biological techniques and the target DNA amplified by PCR using primer pairs C_s/S_{as} (C^{139}, C^{164}) and S_s/C_{as} (W^{207}). Clones displaying the strongest QC expression (Western Blot analysis or activity measurement) were chosen for large-scale expression.

Large-Scale Expression and Purification. High-cell density fermentation (mQC, hQC, and hQC $C^{139}A/C^{164}A$) and expression in shake flasks (hQC $W^{207}F/L/Q$) were used for large-scale expression. Fermentation was conducted in a 5 L reactor (Biostad B; B. Braun Biotech, Melsungen, Germany) as described previously,[18] whereas large-scale shake flask expression was performed with a final volume of 4 L. Before the change from BMGY to BMMY was made, the OD_{600} was adjusted to 1. Cells were grown for 68 h and separated from the medium by centrifugation at 6000*g* and 4 °C for 20 min. The pH was adjusted to 7.0 by addition of saturated Tris buffer and the resulting turbid solution centrifuged at 16000*g* for 30 min at 4 °C.

For purification of human QC, histidine was added to a final concentration of 1 mM and the supernatant applied to an expanded bed adsorption column in the upward flow direction (Streamline Chelating Sepharose, 2.5 cm × 22 cm settled, GE Healthcare, Uppsala, Sweden). The matrix was saturated with Ni^{2+} ions and equilibrated with 50 mM sodium phosphate buffer (pH 6.8) and 300 mM sodium chloride. Bound enzyme was washed with 1.5 L of 50 mM sodium phosphate buffer (pH 6.8) and 300 mM sodium chloride. Human QC was eluted in the downward flow direction at a flow rate of 8 mL/min using 50 mM phosphate buffer (pH 6.8) and 300 mM sodium chloride containing 100 mM histidine. QC-containing fractions were pooled, and ammonium sulfate was added to a final concentration of 700 mM. After centrifugation at 100000*g* (4 °C) for 1 h, the resulting solution was applied to a Butyl Sepharose Fast Flow column (1.6 cm × 13 cm, GE Healthcare) at a flow rate of 2 mL/min. Bound enzyme was washed with 3 column volumes of 50 mM sodium phosphate buffer (pH 6.8) and 700 mM ammonium sulfate and eluted in the reversed flow direction using 5 mM sodium phosphate buffer (pH 6.8). Fractions containing QC activity were pooled and dialyzed overnight at 4 °C against a 100-fold (v/v) excess of 30 mM Bis-Tris (pH 6.8). The solution was centrifuged at 100000*g* (4 °C) for 1 h and applied to an Uno Q6 column (12 mm × 53 mm, Bio-Rad) at a flow rate of 4 mL/min. Bound enzyme was washed with 3 column volumes of 30 mM Bis-Tris (pH 6.8). Human QC was eluted with 30 mM Bis-Tris (pH 6.8) containing 360 mM sodium chloride. QC-containing fractions were pooled, and the purity was analyzed by sodium dodecyl sulfate−polyacrylamide gel electrophoresis (SDS−PAGE) (Servagel TG 4-20, Serva, Heidelberg, Germany) and Coomassie Blue staining (Figure S1 of the Supporting Information). The purified enzyme was stored at −20 °C after addition of 50% (v/v) glycerol or without glycerol at −80 °C.

Murine QC was purified as described elsewhere, applying cation exchange and hydrophobic interaction chromatography steps.[15] The purified murine QC was finally applied to a HiPrep desalting column (2.6 cm × 10 cm; GE Healthcare) equilibrated with 15 mM Bis-Tris (pH 6.8) containing 100 mM sodium chloride. The homogeneous enzyme preparation was stored at −80 °C.

Circular Dichroism (CD) Spectroscopy. CD spectra were recorded with a Jasco J-715 spectropolarimeter (Jasco, Gross-Umstadt, Germany) using quartz cuvettes with a 0.1 cm path length and an external thermostat (Julabo F25, Julabo, Seelbach, Germany). Buffer exchange of purified QC with 10 mM potassium phosphate buffer (pH 6.8) was performed. For wavelength scans, the mean of 10 scans between 190 and 260 nm (far-UV/amide region) was calculated and corrected by subtraction of the buffer spectrum. To study the thermal stability of WT hQC and

the mutants ($C^{139}A/C^{164}A$ and $W^{207}A/F/L/Q$), the temperature was increased from 20 to 80 °C. Wavelength scans were taken every 10 K, whereas the ellipticity at a wavelength of 227 nm was measured every 2 K. At this wavelength, a major change in the spectrum was observed.

Fluorescence Spectroscopy. To investigate the conformational stability of WT hQC and the $C^{139}A/C^{164}A$ variant, fluorescence emission spectra were recorded in the wavelength range between 320 and 400 nm at 22 °C using the luminescence spectrometer (model LS 50 B, Perkin-Elmer, Waltham, MA) and an excitation wavelength of 295 nm. Human QC (0.24 μM) and hQC $C^{139}A/C^{164}A$ (0.31 μM) were dissolved in 50 mM sodium phosphate buffer (pH 6.8) containing GdmCl (guanidinium hydrochloride) in the concentration range of 0−6 M. Spectra were recorded, and the spectrum of the corresponding buffer was subtracted.

QC Enzymatic Assays. QC activity was assayed in 50 mM Tris-HCl (pH 8.0) essentially as described previously.[21] For spectrophotometric measurements, samples contained 30 units/mL glutamic dehydrogenase, 0.25 mM NADH/H^+ (nicotinamide adenine dinucleotide), and 15 mM α-ketoglutaric acid. Reactions were started by the addition of QC, and activity was monitored by recording the decrease in absorbance at 340 nm.

For the fluorometric detection of QC activity, reaction mixtures contained the substrate [H-Gln-βNA (β-naphthylamide) or H-Gln-AMC (7-amino-4-methylcoumaride)] and 0.4 unit/mL pyroglutamyl aminopeptidase as the auxiliary enzyme. The excitation and emission wavelengths were 380 and 460 nm (H-Gln-AMC) or 320 and 410 nm (H-Gln-βNA), respectively. Reactions were started by addition of QC. QC activity was determined from a standard curve of the fluorophore under assay conditions. All determinations were conducted at 30 °C using the BMG Fluostar microplate reader (BMG Labtechnologies, Offenburg, Germany).

For inhibitor testing, the same sample composition was used as described above, except for the added inhibitory compound. Inhibitory constants were determined using H-Gln-AMC in a concentration range between $0.25K_m$ and $4K_m$. Evaluation of all kinetic data was performed using GraFit (version 5.0.4 for Windows, Erithacus software Ltd., Horley, U.K.).

Protein Crystallization. Crystals were grown using the hanging drop vapor diffusion technique at room temperature (21 °C) in Easyxtal 24-well plates (Qiagen). Recombinant glycosylated hQC was concentrated to 10 mg/mL in the presence of 25 mM Bis-Tris (pH 6.8) and 100 mM sodium chloride and mixed at a ratio of 1 μL of protein solution to 1 μL of crystallization buffer. Platelike crystals grew within 10−15 days in 100 mM imidazole (pH 8), 30% (v/v) 2-methyl-2,4-pentanediol, and 11% (w/v) 4000 PEG.

Recombinant mQC was concentrated to 10 mg/mL in 15 mM Bis-Tris (pH 6.8) and 100 mM sodium chloride and mixed with an equal volume of crystallization buffer. To obtain cocrystals, the concentrated protein was mixed together with the inhibitor PQ50 (final concentration of 1 mM) prior to crystallization. Rod- and needle-shaped crystals appeared in the presence of 100 mM sodium acetate (pH 5.3), 200 mM ammonium sulfate, and 12% (w/v) 2000 MME-PEG in the course of 1 week.

Data Collection and Processing. Prior to X-ray measurements, crystals were rapidly soaked with new cryo-buffer solution consisting of mother liquor and 20% (v/v) glycerol. Crystals were collected from the cryo-buffer solution using a pin nylon

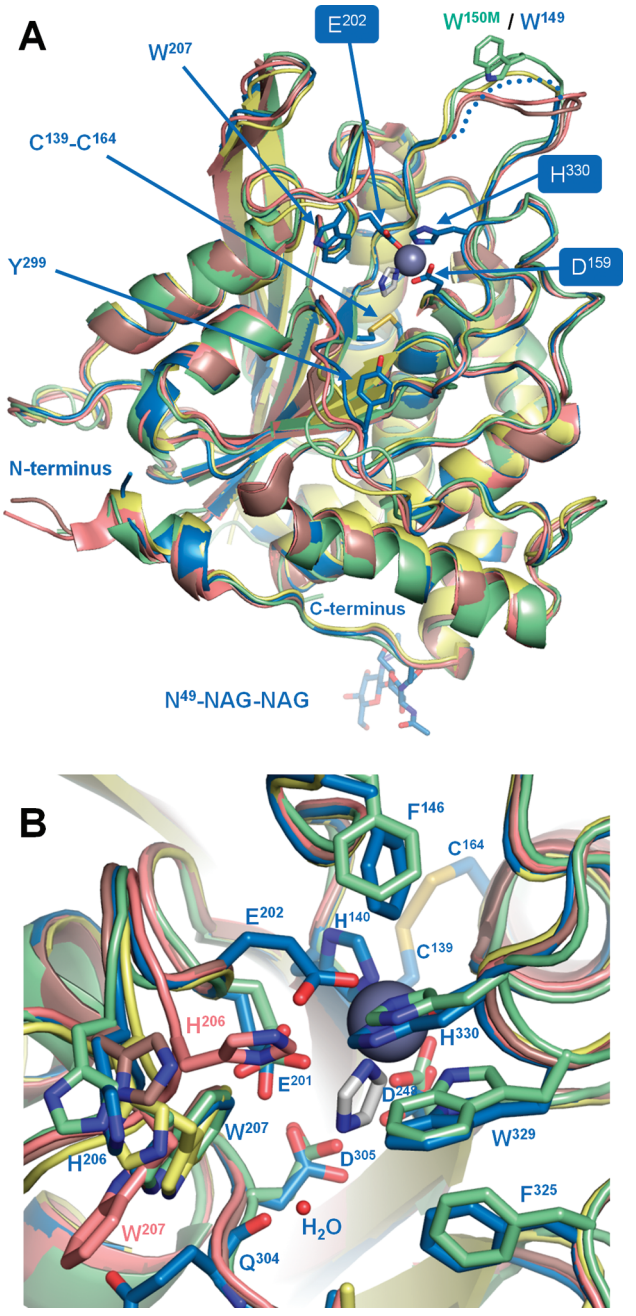

Figure 1. Structures of mammalian QCs. (A) Overall structures of glycosylated human (blue) and murine (green for free mQC and yellow for the complex with PQ50) QCs expressed in *P. pastoris* superimposed on those of human QC produced in *E. coli* (PDB entry 2AFO; pink for molecule A and brown for molecule B).[5] The gray sphere represents the catalytic zinc ion from glycosylated hQC, liganded by the catalytically important residues D^{159}, E^{202}, and H^{330} and the imidazole molecule (white sticks) from the crystallization buffer. The $C^{139}-C^{164}$ disulfide bridge and the N-linked *N*-acetylglucosamine moieties attached to Asn^{49} are depicted as sticks. Loops surrounding the active center that exhibit divergent structure are marked by the included side chains W^{150M}, W^{207}, and Y^{299}. Dotted lines indicate that there was no electron density for these residues. (B) Close-up of the active center, oriented by a rotation of ∼90° about the horizontal axis. Residues that adopt different conformations in the various structures are depicted as sticks. Note the proximity of the disulfide bridge to the active center, as well as the alternative conformations of H^{206} and W^{207}.

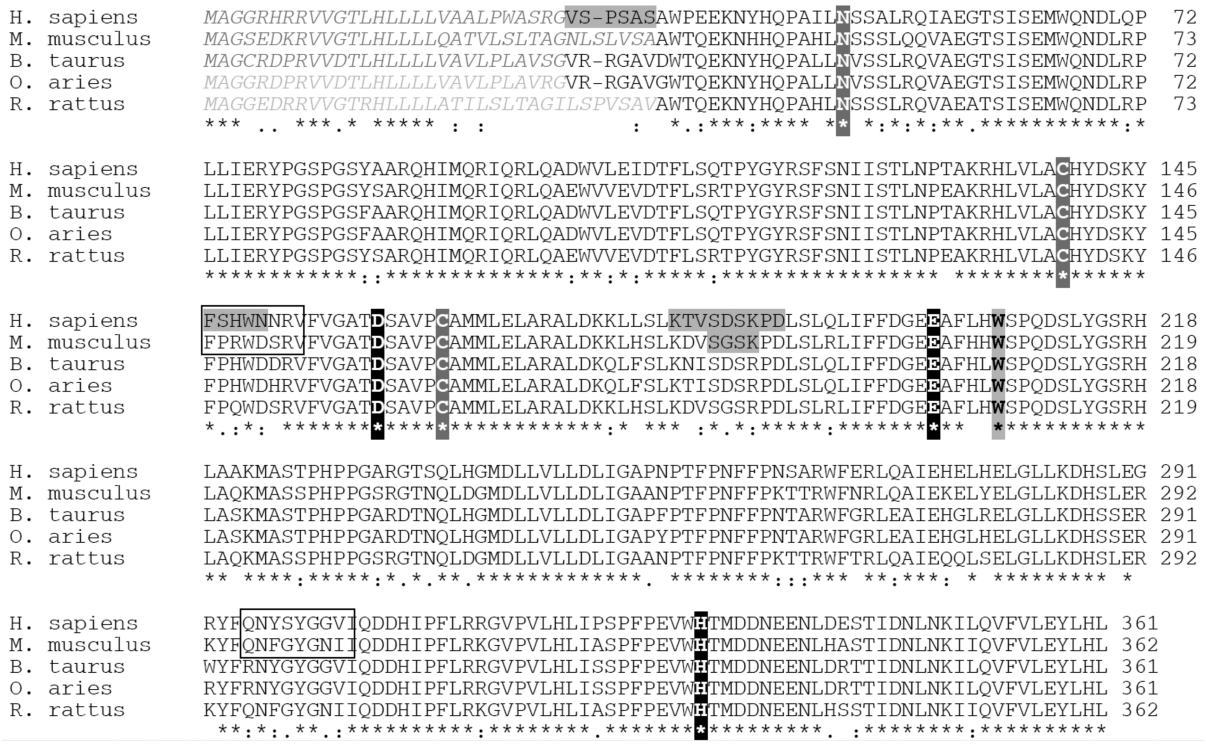

Figure 2. Sequence alignments of human (hQC; UniProt entry Q16769), murine (mQC; UniProt entry Q9CYK2), bovine (*Bos taurus*; UniProt entry Q28120), ovine (*Ovis aries*; UniProt entry C8BKD8), and rat (*Rattus rattus*; UniProt entry D4A1C7) glutaminyl cyclases. Multiple-sequence alignment was performed using ClustalW at ebi.ac.uk with default settings. Zn^{2+} liganding residues (D^{159}, E^{202}, and H^{330}) of the active center are indicated by a black background. The N-glycosylation sites and the disulfide bond-forming cysteine residues, located in a highly conserved region close to the active center, are depicted in white with a gray background. The highly conserved W^{207} (hQC) is shown in bold with a gray background. Surface loops that show altering conformations in the individual structures are boxed, and residues for which no electron density is present are shown with a gray background. Secretion signals are shown in gray italics; putative ovine and rat signal sequences are by analogy to those of bovine and mouse QCs, respectively.

loop, mounted onto the goniometer and flash-frozen at −180 °C using an X-Stream cryo-nitrogen stream (Rigaku/MSC). In house, single-crystal data collection was performed by means of a rotating-anode X-ray source (RA Micro 007, Rigaku/MSC) equipped with a CCD detector device (CCD Saturn 944+, Rigaku/MSC) mounted on an AFC-11 goniometer with VarimaxTM Optics (Rigaku/MSC) using Cu Kα radiation (λ = 1.5418 Å). Crystals were unmounted and stored in liquid nitrogen for subsequent measurement at the BESSY synchrotron in Berlin (beamline BESSY-MX BL14.1) at a wavelength of 0.91841 Å. Data processing was conducted using programs of the CCP4 crystallographic suite.[22] Reflection intensities were indexed and integrated using MOSFLM[22] and scaled and merged using SCALA.[22]

hQC crystals belong to monoclinic space group *C*2 with the following cell constants: a = 82.4 Å, b = 63.6 Å, c = 77.1 Å, and β = 105.7°. They contain one molecule in the asymmetric unit and diffract to 2.08 Å. Initial phases for the hQC structure were obtained by molecular replacement using PHASER and Protein Data Bank (PDB) entry 2AFO (molecule A)[5] as a search model. Manual rebuilding and maximum-likelihood refinement cycles were performed using COOT and REFMAC5 as implemented in the CCP4 suite.[22] The final model, consisting of residues E^{38}−L^{361} (with breaks in the density from F^{146} to N^{150} and K^{182} to D^{190}), could be refined to R_{work} and R_{free} values of 20.5 and 26.3, respectively.

The refined hQC structure was used to determine the mQC structures, which crystallized in orthorhombic space group $P2_12_12_1$ and diffracted to 2.90 Å (1.80 Å) with the following cell constants: a = 43.2 Å, b = 86.9 Å, and c = 97.2 Å (a = 42.7 Å, b = 83.0 Å, and c = 95.7 Å for the mQC−PQ50 complex). These crystals also contain one molecule in the asymmetric unit, and electron density is defined for residues A^{36}−V^{185} and P^{190}−L^{361}. In the unliganded form, residues Q^{295}−I^{303} show weak but interpretable density, while these residues are clearly defined in the mQC−PQ50 complex. Complete data collection and refinement statistics are listed in Table S3 of the Supporting Information.

RESULTS

Crystal Structures of Human and Murine QC Expressed in *P. pastoris*. The hQC and mQC structures presented here exhibit highly similar tertiary structures (rmsd for all Cα atoms of 0.541 Å). As described previously,[5] the proteins possess a globular α/β-hydrolase fold[23] (Figure 1A) with an approximate diameter of 40 Å. A twisted central β-sheet, formed by five parallel (β_1 and β_3−β_6) β-strands and one antiparallel (β_2), is sandwiched by α-helices, with three helices (α_6, α_7, and α_9) filling the concave face and six helices (α_2−α_5, α_8, and α_{10}) shielding the convex face of the blade. The β-sheet is sealed on its vertex by an additional α-helix situated on the N-terminal side of the polypeptide chain (α_1).

The active center of each QC, which is located at the bottom of a pocket whose walls are defined mainly by the side chains of

W^{207} and W^{329} (unless indicated otherwise by the suffix M, residue numbering in this paper refers to that of human QC; the corresponding residue numbers for murine QC are obtained by the addition of 1), accommodates a catalytic zinc ion coordinated by residues D^{159} (OD2), E^{202} (OE2), and H^{330} (NE2). In the unliganded mQC structure, the fourth zinc coordination site is occupied by a water molecule; in the hQC crystal structure (Figure 1B), this position is taken up by an imidazole molecule from the crystallization buffer that interacts with the main chain Q^{304} carbonyl function via a bridging water molecule. The zinc ion is essential for catalytic activity as well as several adjacent conserved amino acid residues, namely, E^{201}, D^{248}, and D^{305}.[17] In agreement with previous studies,[5] the peptide bond between residues D^{159} and S^{160} is in the *cis* conformation in each structure presented here; the *cis* conformer appears to be stabilized via a hydrogen bond network involving D^{248}, a residue also implicated in catalysis.[17]

The location of the N-linked glycosylation site N^{49} (for which clear electron density is present for the first two or three sugars) suggests that the sugar chain should have no direct effect on catalytic activity and is presumably responsible for improved solubility. Superposition of the glycosylated QC structures presented here with those published previously[5] reveals four structurally divergent regions in the neighborhood of the active center (Figure 1). (i) Adjustments are seen in the side chain orientation of the two tryptophan residues, W^{207} and W^{329}. The loop containing W^{207} appears to be influenced by the crystallographic environment of the preceding H^{206}. In each of these structures, these residues adopt an orientation matching that of the "B" molecule reported by Huang et al.[5] (ii) Each QC structure reveals the presence of a disulfide bridge between conserved cysteine residues C^{139} and C^{164} (Figure 2) not formed in previous crystal structure determinations. This disulfide bridge connects strand β_3 and helix α_5 and is located immediately below the active center metal ion. (iii) Residues F^{146}–V^{153} show variable conformations and are for the most part undefined in our hQC structure. (iv) The loop segment of residues Q^{295}–I^{303} shows a variable conformation. Whereas the hQC structure shows minor differences in this loop with respect to earlier structures, the mQC structures deviate considerably; indeed, this region is relatively poorly defined in the absence of ligand, while it adopts a clear and alternative conformation in cocrystals with PQ50 (see below).

Role of the Conserved Disulfide Bond in hQC. To address the role of the conserved disulfide bond in human and murine QC, whose importance in creating a catalytic active QC structure was suggested in previous studies,[18] we replaced both cysteines with alanine. Analysis of the catalytic parameters k_{cat}/K_m, k_{cat}, and K_m for conversion of different substrates by the wild type (WT) and the mutant $C^{139}A/C^{164}A$ revealed only a minor influence of the disulfide bond on catalysis (Figure 3A). The k_{cat}/K_m ratios between mutant and WT hQC were close to 1, with maximal deviations of the substrate specificity of $0.5(k_{cat}/K_m)_{WT}$ (H-Gln-Glu-OH) and $4.2(k_{cat}/K_m)_{WT}$ (H-Gln-Phe-Ala-NH_2). Similarly, the enzyme–inhibitor interaction was not affected significantly, with only a small increase in the K_i ratio for PQ50 ($2.7K_{iWT}$) and cysteamine ($1.5K_{iWT}$) (Figure 3B; kinetic parameters for the WT enzyme provided in Tables S4 and S5 of the Supporting Information), arguing against a direct role for the disulfide bond in the formation of a catalytically active structure.

To investigate a potential stabilizing role of the disulfide bond, the thermal unfolding of WT hQC and the $C^{139}A/C^{164}A$ mutant

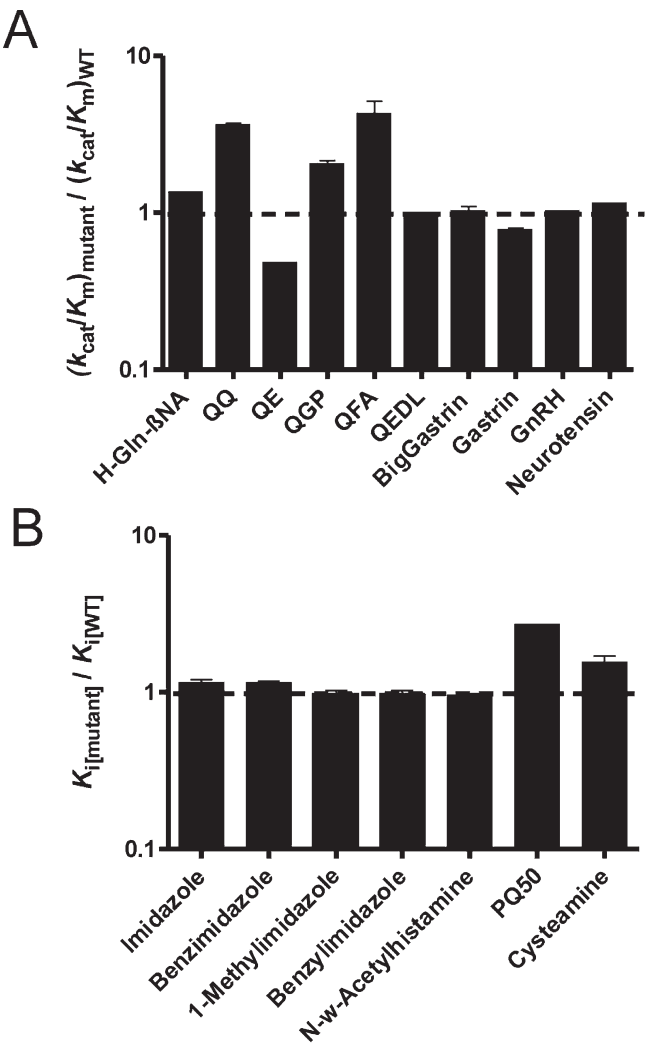

Figure 3. Enzyme kinetic characterization of hQC and its variant $C^{139}A/C^{164}A$. (A) Ratio of the substrate specificities of the $C^{139}A/C^{164}A$ mutant and WT hQC, $(k_{cat}/K_m)_{mutant}/(k_{cat}/K_m)_{WT}$. A ratio close to unity suggests that the disulfide bridge does not exert a direct influence on enzyme activity. (B) Ratio of the inhibitory constants of the $C^{139}A/C^{164}A$ mutant and WT hQC, $K_{i[mutant]}/K_{i[WT]}$. The enzyme–inhibitor interaction is barely influenced by the disulfide bond. Reactions were conducted in 50 mM Tris (pH 8.0) at 30 °C; ratios ± the standard deviation were calculated from three independent measurements.

was assessed using far-UV CD spectroscopy (Figure 4A and Figure S2 of the Supporting Information). All transitions show a sigmoidal shape, with inflection points for WT and $C^{139}A/C^{164}A$ variant enzymes of 49 and 46 °C, respectively, pointing to a destabilization of the protein as a result of the mutation. In the absence of metal ions, this effect is even more pronounced, with the inflection points shifting to 36 and 30 °C for apoWT and apo$C^{139}A/C^{164}A$ QC, respectively.

Fluorescence spectroscopy of QC denaturation using GdmCl corroborated these results. The metal-bound enzymes (WT hQC and the $C^{139}A/C^{164}A$ mutant) exhibit a fluorescence emission maximum at 344 nm that shifts to 354 nm upon unfolding, indicating a more hydrophilic environment of the tryptophan residues compared to the folded state (Figure S3 of the Supporting Information).[24] While the conformation of both

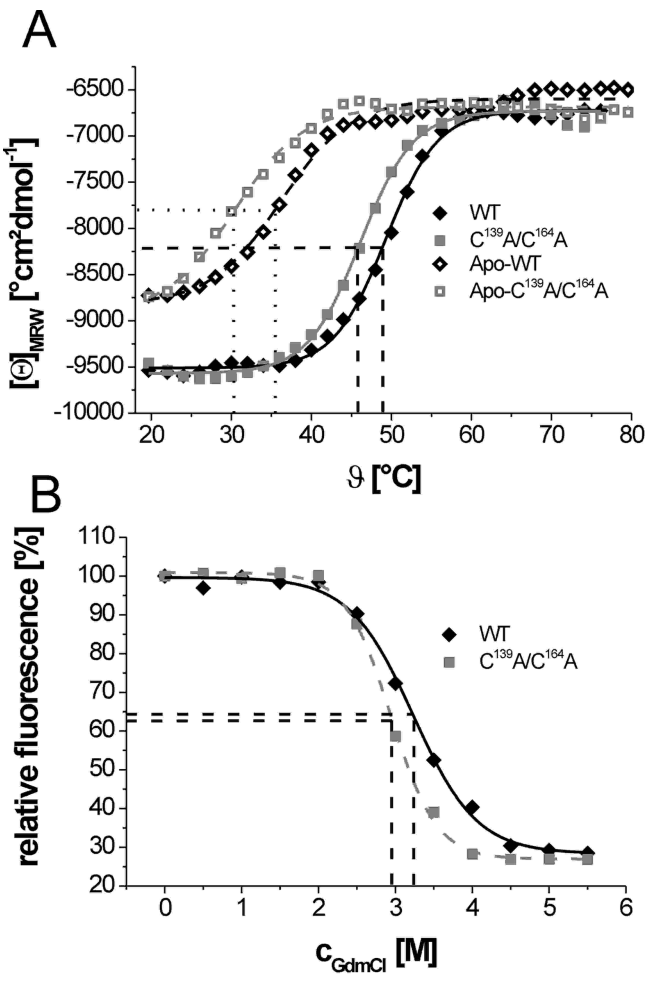

Figure 4. Conformational stability of WT hQC and hQC variant $C^{139}A/C^{164}A$. (A) Thermal unfolding of WT hQC and hQC $C^{139}A/C^{164}A$ observed as a temperature-dependent change in the mean residue ellipticity (θ_{MRW}) at 227 nm, as well as corresponding apo forms lacking the catalytic zinc ion[14,25] (empty symbols). Data evaluation according to a sigmoidal model reveals inflection points of 49.3 ± 0.1 and 46.1 ± 0.1 °C for the WT and the variant, respectively. The apoenzymes showed a notable decrease in thermal stability, marked by medial transition temperatures of 36.2 ± 0.5 and 30.4 ± 0.5 °C, respectively. Proteins were dissolved in 10 mM potassium phosphate buffer (pH 6.8). (B) GdmCl-mediated unfolding of WT hQC and hQC variant $C^{139}A/C^{164}A$ monitored by changes in relative fluorescence emission at 337 nm. Inflection points of the sigmoidal curves for WT hQC and the $C^{139}A/C^{164}A$ variant were 3.2 and 2.9 M, respectively. Proteins were dissolved in 50 mM sodium phosphate buffer (pH 6.8), and data collection was conducted at 22 °C and an excitation wavelength of 295 nm.

enzymes is stable at a GdmCl concentration of up to 2 M, unfolding of the hQC variant $C^{139}A/C^{164}A$ proceeds rapidly, with an inflection point of 2.9 M compared to 3.2 M for WT hQC. At 4 M GdmCl, WT hQC still possesses a significant folded fraction, whereas the disulfide-less mutant is completely unfolded (Figure 4B). Thus, both thermal and chemical unfolding analyses support a conformation-stabilizing effect of the disulfide bond.

Relevance of W^{207} for Catalysis and Enzyme−Inhibitor Interactions. Steady-state kinetic parameters K_m and k_{cat} of hQC variants $W^{207}F$, $W^{207}L$, and $W^{207}Q$ were determined for the conversion of H-Gln-βNA, H-Gln-Gln-OH, H-Gln-Glu-OH, H-Gln-Phe-Ala-NH_2, H-Gln-Gly-Pro-OH, and H-Gln-Glu-Asp-Leu-NH_2 (Table S4 of the Supporting Information) and their specificity constants k_{cat}/K_m plotted as a ratio of hQC mutant to wild type (Figure 5A). Each replacement of W^{207} reduces substrate specificity by a combined increase in the Michaelis−Menten constant and decrease in the turnover number (Figure S4 of the Supporting Information). The latter decrease in the k_{cat} value is independent of the substrate and is influenced only slightly by the nature of the substituted side chain. In contrast, the increase in the Michaelis−Menten constant is dependent on the size and polarity of the exchanged amino acid. While replacing W^{207} with phenylalanine does not exert a significant influence on K_m (maximal $3K_{mWT}$), introduction of an aliphatic ($W^{207}L$) or polar (Q) amino acid results in K_m values more than 10-fold greater than K_{mWT} (Figure S4 of the Supporting Information). These results indicate that, even if W^{207} is not directly involved in the catalytic process through, for example, substrate positioning, there is at least a stabilizing function for optimal catalytic activity. No influence of W^{207} exchange on thermal stability could be detected (Figure S5 of the Supporting Information).

In contrast to substrate conversion, the interaction with small inhibitors (imidazole, benzimidazole, or methylimidazole) is not influenced by exchange of W^{207} (Figure 5B and Table S5 of the Supporting Information). For larger inhibitors such as benzylimidazole, *N*-ω-acetylhistamine, and PQ50, differences in the K_i ratio are observed that depend on the kind of amino acid replacement. While the inhibition of hQC variant $W^{207}F$ remains like that of the wild type, the inhibition of variants $W^{207}L$ and -Q decrease by a factor of up to 10, suggesting that W^{207} may be involved in secondary interactions with these inhibitors.

Binding Mode of the Specific Inhibitor PQ50. The imidazole group of PQ50 occupies a deep pocket (Figure 6A) whose walls are restricted by the side chains of W^{208M}, I^{304M}, F^{326M}, and W^{330M} and can be superimposed on the free imidazole molecule observed in the hQC structure. The free nitrogen atom of the inhibitor imidazole moiety engages the fourth coordination site of the zinc cation, occupied in free mQC by a water molecule. The PQ50 propyl linker passes through the narrow restriction; a water-mediated hydrogen bond is observed between the thiourea N1 atom and the backbone amide of Q^{305M}, whereas the thiocarbonyl group itself is exposed to bulk solvent. The phenyl moiety rests upon the wide valleylike active center cleft opening, with its aromatic ring covering the hydrophobic side chain of I^{304M}, and the two methoxy groups are involved in van der Waals interactions with the protein surface. Although there do not appear to be any major rearrangements of mQC residues in direct contact with the inhibitor, the loop segment of N^{297M}−I^{303M} adopts an alternative conformation compared to free mQC, which may be due to a potential clash between the carbonyl group of I^{303M} and the PQ50 aromatic moiety.

DISCUSSION

Glutaminyl cyclases are thought to play a pivotal role in the maturation of neuropeptides such as GnRH or TRH. Indeed, a recent characterization of QC knockout mice revealed a mild influence on the hypothalamic−pituitary−thyroid (HPT) axis but, surprisingly, not on the hypothalamic−pituitary−gonadal (HPG) axis.[26] Although the reason for the differential substrate conversion of GnRH and TRH remains to be clarified, this might be due to partial compensation of GnRH maturation by a ubiquitous isoenzyme of QC. As the knockout of QC does not

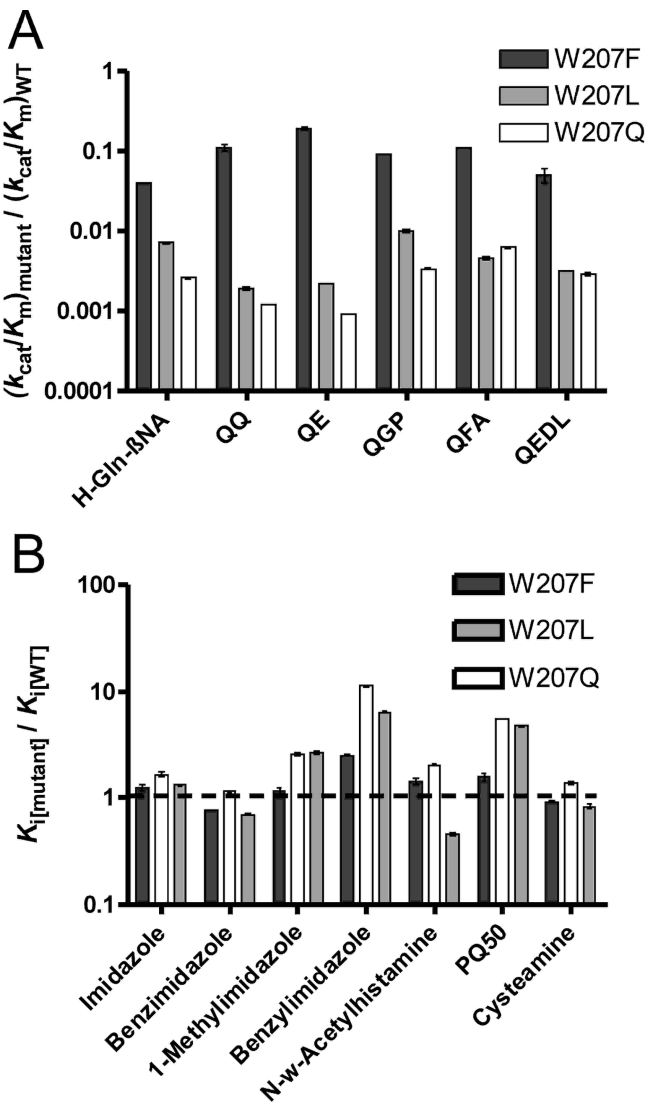

Figure 5. Enzyme kinetic characterization of WT hQC and hQC variants W^{207}F, -L, and -Q. (A) Ratio of the substrate specificities of W^{207} variants and WT hQC, $(k_{cat}/K_m)_{mutant}/(k_{cat}/K_m)_{WT}$. An exchange of W^{207} results in a significant reduction in the specificity constant caused by a decreased turnover number (k_{cat}) as well as an increased Michaelis−Menten constant (K_m) (cf. Figure S4 of the Supporting Information). (B) Ratio of the inhibitor constants of W^{207} variants and WT hQC, $K_{i[mutant]}/K_{i[WT]}$. Inhibitors that interact with the enzyme primarily via the active center zinc ion (imidazole, benzimidazole, and cysteamine) are not affected by exchange of W^{207}, whereas the larger benzylimidazole, *N*-ω-acetylhistamine, and PQ50 show an increased ratio, indicating that W^{207} should be involved in secondary interactions. Reactions were conducted in 50 mM Tris (pH 8.0) at 30 °C; ratios ± the standard deviation were calculated from three independent determinations.

result in any behavioral or developmental phenotype, current efforts to develop QC inhibitors to suppress pGlu-amyloid toxicity in neurodegenerative disorders appear feasible.[13]

We have therefore undertaken the structural determination of human and murine QCs as a first step in the development of novel inhibitors. As anticipated, the two enzymes are highly convergent in structural terms, and in particular, their active centers and the approaches thereto are virtually identical. Utilization of the yeast secretory pathway for protein expression allowed the analysis of two potentially important QC enzyme modifications (N-glycosylation and disulfide formation) and revealed no significant changes in the overall structures of the two mammalian QCs, reflected by a lack of influence on catalytic activity. On the other hand, deletion of the disulfide bond, conserved in all mammalian QCs (Figure 2), leads to a substantial decrease in protein stability, which is exacerbated by removal of the catalytic metal ion. Presumably, this stabilization of the catalytically active structure has led to conservation of the disulfide bridge.

Our structural studies reveal plasticity in the loops surrounding the active center, namely, F^{146}−V^{153}, H^{206}-W^{207}, and Q^{295}−I^{303}. Previous studies[5] had shown that the side chain of W^{207} can adopt (at least) two different orientations. Our results confirm an influence of this residue upon the catalytic activity of hQC; mutation presumably causes changes in the microenvironment of the catalytic center as suggested by the simultaneous increase in K_m and decrease in k_{cat} values. While the observed loop rearrangements have no effect on the binding of inhibitors even as large as PQ50, these may be important for macromolecular substrate recognition. Interestingly, we observed a similar malleability of residues surrounding the active center cleft of the evolutionarily unrelated microbial QCs recently.[8]

Finally, we have delineated the binding mode of the potent inhibitor PQ50 in murine QC. Residues involved in binding the inhibitor are identical in both human and murine QCs; a potential clash between the methoxy group of PQ50 and the side chain hydroxyl of human QC Y^{299} (not shown) could easily be accommodated by a minor rotation of the aromatic group of the inhibitor, although it should be borne in mind that the loop containing Y^{299} appears to exhibit a natural flexibility. During the final stages of preparation of our manuscript, the structure of PQ50 in complex with hQC (Figure 6B) was reported.[27] Whereas the imidazole headgroup occupies identical positions in murine and human QCs, striking differences are seen in the orientation of the thiourea and aromatic moieties. Through a rotation of 90°, the thio-carbonyl group forms a direct hydrogen bond with the backbone amide of Q^{304} in hQC, replacing the (conserved) water molecule that in mQC hydrogen bonds to both Q^{305M} and the thiourea N1 atom. The aromatic moiety covers a similar hydrophobic patch in each enzyme, but the two methoxy groups are involved in solvent-mediated hydrogen bonds to the backbone amide of F^{325}.

These differences raise an obvious question. Which binding mode corresponds to the "correct" protein−inhibitor interaction? In both structures (obtained via cocrystallization experiments), crystal contacts in the neighborhood of PQ50 could well influence the binding mode. While crystals of human isoQC soaked with PQ50[27] reveal interactions equivalent to those seen for hQC, structure−activity relationships (SARs) of related compounds[28,29] provide important clues (Figure S6 of the Supporting Information). Whereas variations in the imidazole moiety (where an additional methyl group in position 5 can provide additional hydrophobic contacts and thereby fix the group for enhanced zinc binding, compounds 9** and 11** in Figure S6) and the propyl linker (whose length appears to be optimal, compounds 54* and 55*) do not differentiate between the two binding modes, the nature of the functional group between the alkyl and aryl parts of this class of inhibitor appears to play an important role in the interaction, with the thiourea group conferring the greatest potency. The SAR indicates that the hydrogen bond donors (N1 and N3) are more important than the acceptor (S vs O, compound 51*) and that the N1 atom is essential (compounds 70*, 81*, and 85*), providing support for

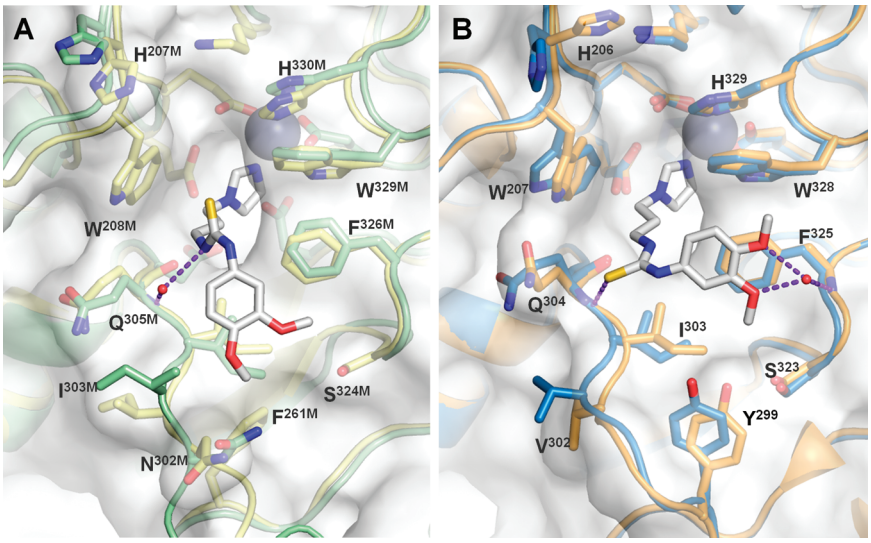

Figure 6. Binding mode of the potent QC inhibitor PQ50 in the active center of (A) murine QC (yellow; other colors as in Figure 1) and (B) human QC (orange).[27] (A) The imidazole moiety of the inhibitor binds to the catalytic zinc ion at the base of a deep cavity whose walls are formed by the hydrophobic side chains W^{208M}, I^{304M}, F^{326M}, and W^{330M} (note that the numbering refers to murine QC, which differs by 1 with respect to that of human QC). The thiourea group makes a water-mediated hydrogen bond to the backbone amide of Q^{305M}, and the phenyl moiety rests upon a hydrophobic patch on the surface of the enzyme. Apparently, the loop segment of N^{297M}–I^{303M} reorganizes concomitantly with inhibitor binding (cf. the structure of free mQC, colored green). (B) Whereas binding of the imidazole headgroup to the active site of hQC is more or less identical to that in mQC, there are significant differences in the orientation of the thiourea group (whose thio-carbonyl moiety is within hydrogen bonding distance of the Q^{304} backbone amide) and the positioning of the dimethoxyphenol moiety (where both methoxy groups are involved in water-mediated hydrogen bonds to the backbone amide of F^{325}). Note that hQC also shows a slight structural reorganization compared with the imidazole-ligated hQC (blue), and that upon appropriate minor side chain rearrangements, the inhibitor could access both binding modes in each enzyme.

the binding mode seen in murine QC. On the other hand, the SAR depends strongly on substituents on the aromatic ring: the substantial effect observed upon removal of one (compound 44*) or both (compound 33*) methoxy groups lends more support to the interaction displayed in crystals of human QC. The structure-based interpretation of inhibition data is, however, notoriously difficult in cases where the inhibitor binding site is flexible;[30] it is quite possible that both observed binding modes are adopted in solution, which may even provide favorable entropic contributions to affinity.

In summary, we present here the first structural analyses of glycosylated mammalian QCs. Although the post-translational modifications (N-glycosylation and disulfide formation) have no direct effect on the enzyme structure or activity, they do influence solubility and stability, perhaps accounting for previously reported differences between QC enzymes expressed in yeast and *E. coli*.[18] Knowledge of the observed active center structural variability allows a broader analysis of possible productive in silico inhibitory binding modes, allowing the prediction, development, and screening of advanced QC inhibitors.

■ ASSOCIATED CONTENT

Supporting Information. Comparison of the kinetic parameters of human QC recombinantly expressed by different systems (Table S1), oligonucleotides applied for cloning and mutation of WT hQC and its variants (Table S2), characterization of WT hQC and its mutants by SDS–PAGE (Figure S1), summary of data set statistics for crystals of human and mouse QC and their corresponding data processing and model building (Table S3), far-UV CD spectra (190 nm < λ < 260 nm) of WT hQC and hQC variant $C^{139}A/C^{164}A$ lacking the disulfide bond (Figure S2), fluorescence emission spectra (320 nm < $\lambda_{emission}$ < 400 nm) of (A) WT hQC and (B) hQC variant $C^{139}A/C^{164}A$ lacking the disulfide bond at increasing concentrations of GdmCl (Figure S3), kinetic constants for WT hQC substrates (Table S4), catalytic parameters of hQC variants $W^{207}F$, -L, and -Q (Figure S4), far-UV CD spectra (190 nm < λ < 260 nm) of WT hQC and the W^{207} variants (Figure S5), inhibitory constants for WT hQC (Table S5), and SARs for PQ50 (Figure S6) (data and compound numbers taken from refs 28 and 29). This material is available free of charge via the Internet at http://pubs.acs.org.

■ AUTHOR INFORMATION

Corresponding Author

*S.S.: Probiodrug AG, Weinbergweg 22, D-06120 Halle (S), Germany; telephone, +49 345 5559900; fax, +49 345 5559901; e-mail, Stephan.Schilling@probiodrug.de. M.T.S.: Institut für Biochemie and Biotechnologie, Martin-Luther-Universität Halle-Wittenberg, Kurt-Mothes-Strasse 3, D-06120 Halle (S), Germany; telephone, +49 345 55 24901; fax, +49 345 55 27360; e-mail, stubbs@biochemtech.uni-halle.de.

Author Contributions

D.R.C. and B.K. contributed equally to this work.

Funding Sources

This work was supported in part by ProNet-T^3 (Protein-Kompetenznetzwerk-Halle: Tools, Targets and Therapeutics) of the German Bundesministerium für Bildung und Forschung (BMBF) Initiative "Spitzenforschung und Innovation" as well as BMBF grant #3013185 to probiodrug AG (H.-U.D.).

■ ACKNOWLEDGMENT

We thank Dr. Uwe Müller (Free University Berlin at BESSY) for synchrotron time.

■ ABBREVIATIONS

hQC, human glutaminyl cyclase; MME-PEG, monomethyl ether polyethylene glycol; mQC, murine glutaminyl cyclase; PCR, polymerase chain reaction; pE, pyroglutamate; rmsd, root-mean-square deviation; SAR, structure−activity relationship.

■ REFERENCES

(1) Busby, W. H. J., Quackenbush, G. E., Humm, J., Youngblood, W. W., and Kizer, J. S. (1987) An enzyme(s) that converts glutaminyl-peptides into pyroglutamyl-peptides. Presence in pituitary, brain, adrenal medulla, and lymphocytes. *J. Biol. Chem. 262*, 8532–8536.

(2) Messer, M., and Ottesen, M. (1965) Isolation and properties of glutamine cyclotransferase of dried papaya latex. *C. R. Trav. Lab. Carlsberg 35*, 1–24.

(3) Messer, M. (1963) Enzymatic cyclization of L-glutamine and L-glutaminyl peptides. *Nature 4874*, 1299.

(4) Messer, M., and Ottesen, M. (1964) Isolation and properties of glutamine cyclotransferase of dried papaya latex. *Biochim. Biophys. Acta 92*, 409–411.

(5) Huang, K. F., Liu, Y. L., Cheng, W. J., Ko, T. P., and Wang, A. H. (2005) Crystal structures of human glutaminyl cyclase, an enzyme responsible for protein N-terminal pyroglutamate formation. *Proc. Natl. Acad. Sci. U.S.A. 102*, 13117–13122.

(6) Azarkan, M., Clantin, B., Bompard, C., Belrhali, H., Baeyens-Volant, D., Looze, Y., Villeret, V., and Wintjens, R. (2005) Crystallization and preliminary X-ray diffraction studies of the glutaminyl cyclase from Carica papaya latex. *Acta Crystallogr. F61*, 59–61.

(7) Huang, W. L., Wang, Y. R., Ko, T. P., Chia, C. Y., Huang, K. F., and Wang, A. H. (2010) Crystal structure and functional analysis of the glutaminyl cyclase from *Xanthomonas campestris*. *J. Mol. Biol. 401*, 374–388.

(8) Carrillo, D. R., Parthier, C., Janckel, N., Grandke, J., Stelter, M., Schilling, S., Boehme, M., Neumann, P., Wolf, R., Demuth, H. U., Stubbs, M. T., and Rahfeld, J. U. (2010) Kinetic and structural characterization of bacterial glutaminyl cyclases from *Zymomonas mobilis* and *Myxococcus xanthus*. *Biol. Chem. 391*, 1419–1428.

(9) Bockers, T. M., Kreutz, M. R., and Pohl, T. (1995) Glutaminyl-cyclase expression in the bovine/porcine hypothalamus and pituitary. *J. Neuroendocrinol. 7*, 445–453.

(10) Pohl, T., Zimmer, M., Mugele, K., and Spiess, J. (1991) Primary structure and functional expression of a glutaminyl cyclase. *Proc. Natl. Acad. Sci. U.S.A. 88*, 10059–10063.

(11) Schilling, S., Hoffmann, T., Manhart, S., Hoffmann, M., and Demuth, H. U. (2004) Glutaminyl cyclases unfold glutamyl cyclase activity under mild acid conditions. *FEBS Lett. 563*, 191–196.

(12) Cynis, H., Schilling, S., Bodnar, M., Hoffmann, T., Heiser, U., Saido, T. C., and Demuth, H. U. (2006) Inhibition of glutaminyl cyclase alters pyroglutamate formation in mammalian cells. *Biochim. Biophys. Acta 1764*, 1618–1625.

(13) Schilling, S., Zeitschel, U., Hoffmann, T., Heiser, U., Francke, M., Kehlen, A., Holzer, M., Hutter-Paier, B., Prokesch, M., Windisch, M., Jagla, W., Schlenzig, D., Lindner, C., Rudolph, T., Reuter, G., Cynis, H., Montag, D., Demuth, H. U., and Rossner, S. (2008) Glutam\inyl cyclase inhibition attenuates pyroglutamate Aβ and Alzheimer's disease-like pathology. *Nat. Med. 14*, 1106–1111.

(14) Schilling, S., Niestroj, A. J., Rahfeld, J.-U., Hoffmann, T., Wermann, M., Zunkel, K., Wasternack, C., and Demuth, H.-U. (2003) Identification of Human Glutaminyl Cyclase as a Metalloenzyme: Inhibition by Imidazole Derivatives and Heterocyclic Chelators. *J. Biol. Chem. 278*, 49773–49779.

(15) Schilling, S., Cynis, H., von Bohlen, A., Hoffmann, T., Wermann, M., Heiser, U., Buchholz, M., Zunkel, K., and Demuth, H. U. (2005) Isolation, catalytic properties, and competitive inhibitors of the zinc-dependent murine glutaminyl cyclase. *Biochemistry 44*, 13415–13424.

(16) Booth, R. E., Lovell, S. C., Misquitta, S. A., and Bateman, R. C., Jr. (2004) Human glutaminyl cyclase and bacterial zinc aminopeptidase share a common fold and active site. *BMC Biol. 2*, 2.

(17) Huang, K. F., Wang, Y. R., Chang, E. C., Chou, T. L., and Wang, A. H. (2008) A conserved hydrogen-bond network in the catalytic centre of animal glutaminyl cyclases is critical for catalysis. *Biochem. J. 411*, 181–190.

(18) Schilling, S., Hoffmann, T., Rosche, F., Manhart, S., Wasternack, C., and Demuth, H. U. (2002) Heterologous expression and characterization of human glutaminyl cyclase: Evidence for a disulfide bond with importance for catalytic activity. *Biochemistry 41*, 10849–10857.

(19) Fischer, W. H., and Spiess, J. (1987) Identification of a mammalian glutaminyl cyclase converting glutaminyl into pyroglutamyl peptides. *Proc. Natl. Acad. Sci. U.S.A. 84*, 3628–3632.

(20) Schilling, S., Manhart, S., Hoffmann, T., Ludwig, H.-H., Wasternack, C., and Demuth, H.-U. (2003) Substrate specificity of glutaminyl cyclases from plants and animals. *Biol. Chem. 384*, 1583–1592.

(21) Schilling, S., Hoffmann, T., Wermann, M., Heiser, U., Wasternack, C., and Demuth, H.-U. (2002) Continuous spectrometric assays for glutaminyl cyclase activity. *Anal. Biochem. 303*, 49–56.

(22) Collaborative Computational Project 4. (1994) The CCP4 suite: Programs for protein crystallography. *Acta Crystallogr. D50*, 760–763.

(23) Carr, P. D., and Ollis, D. L. (2009) α/β hydrolase fold: An update. *Protein Pept. Lett. 16*, 1137–1148.

(24) Schmid, F. X. (1989) in *Protein Structure: A Practical Approach* (Creighton, T. E., Ed.) pp 251−285, Oxford University Press, New York.

(25) Huang, K. F., Liu, Y. L., and Wang, A. H. (2005) Cloning, expression, characterization, and crystallization of a glutaminyl cyclase from human bone marrow: A single zinc metalloenzyme. *Protein Expression Purif. 43*, 65–72.

(26) Schilling, S., Kohlmann, S., Bäuscher, C., Sedlmeier, R., Koch, B., Eichentopf, R., Becker, A., Cynis, H., Hoffmann, T., Berg, S., Freyse, E. J., von Hörsten, S., Rossner, S., Graubner, S., and Demuth, H. U. (2011) Glutaminyl cyclase knock-out mice exhibit slight hypothyroidism but no hypogonadism: Implications for enzyme function and drug development. *J. Biol. Chem. 286*, 14199–14208.

(27) Huang, K. F., Liaw, S. S., Huang, W. L., Chiam, C. Y., Lom, Y. C., Chen, Y. L., and Wang, A. H. (2011) Structures of human Golgi-resident glutaminyl cyclase and its complexes with inhibitors reveal a large loop movement upon inhibitor binding. *J. Biol. Chem. 286*, 12439–12449.

(28) Buchholz, M., Heiser, U., Schilling, S., Niestroj, A. J., Zunkel, K., and Demuth, H. U. (2006) The first potent inhibitors for human glutaminyl cyclase: Synthesis and structure-activity relationship. *J. Med. Chem. 49*, 664–677.

(29) Buchholz, M., Hamann, A., Aust, S., Brandt, W., Böhme, L., Hoffmann, T., Schilling, S., Demuth, H. U., and Heiser, U. (2009) Inhibitors for human glutaminyl cyclase by structure based design and bioisosteric replacement. *J. Med. Chem. 52*, 7069–7080.

(30) Rauh, D., Klebe, G., and Stubbs, M. T. (2004) Understanding protein-ligand interactions: The price of protein flexibility. *J. Mol. Biol. 335*, 1325–1341.